State-Space Harmonic Distortion Modeling in Weakly Nonlinear, Fully Balanced G_m-C Filters—A Modular Approach Resulting in Closed-Form Solutions

Zhaonian Zhang, *Student Member, IEEE*, Abdullah Celik, *Student Member, IEEE*, and Paul P. Sotiriadis, *Member, IEEE*

***Abstract*—State space harmonic distortion modeling and estimation are introduced for G_m-C filters with fully balanced, weakly nonlinear tranconductors. The proposed method provides compact closed-form answers expressed explicitly in terms of the values of the circuit elements. It can be easily implemented in MATLAB and applied to G_m-C filters of any order. The filter is viewed as a composition of three operators in signal space representing the input stage, the filter core, and the output stage. Each operator is then decomposed into the superposition of a linear operator and a nonlinear operator. The total distortion at the output is shown to be approximately the sum of the distortion introduced by the nonlinear operator of each stage. The theoretical results are found to be in good agreement with Cadence simulations for the cases of a lossy integrator and a third-order Butterworth low-pass filter.**

***Index Terms*—Circuit analysis, distortion model, G_m-C filters, fast algorithm, fully balanced, fully differential, harmonic distortion, perturbation, state space, weak nonlinearity.**

I. Introduction

CONTINUOUS-TIME transconductor-capacitor (G_m-C) filters have received significant attention in the past two decades. They have been widely employed in a variety of applications including audio and video applications, telecommunications, and low-power analog systems [1]–[11]. Their tunability, low-power, and high-frequency capability have made them popular in the analog circuits community.

However, to achieve high frequency performance, linearity is often sacrificed in favor of simple and fast transconductor topologies. This results in nonnegligible distortions at the transconductors and therefore at the output of the G_m-C filters.

When a sinusoidal signal of frequency ω is applied to the input of the filter, the steady-state response at the output consists of not only the component at the fundamental frequency ω, but also the components at harmonic frequencies $2\omega, 3\omega, 4\omega, \cdots$. These higher order terms are referred to as *harmonic distortion*. The total harmonic distortion (THD) is defined as

$$\mathrm{THD} = \frac{\sqrt{V_{h2}^2 + V_{h3}^2 + V_{h4}^2 + \cdots}}{V_f} \times 100\% = 20\log_{10}\sqrt{\frac{V_{h2}^2 + V_{h3}^2 + V_{h4}^2 + \cdots}{V_f^2}} \quad (\text{in dB})$$

where V_f is the amplitude of the component at ω and V_{hk} is the amplitude of the component at the kth harmonic $k\omega$, $k = 2, 3, 4, \ldots$.

Harmonic distortion is a major issue in many applications such as antialiasing filters in analog-to-digital converters (ADC). Suppose for example that the input signal to an ADC is a sinusoidal signal at 400 kHz and that the sampling frequency is 1500 kHz. The third-order harmonic component at the output of the antialiasing filter is at 1200 kHz and thus aliased at 300 kHz, which degrades the signal-to-noise ratio (SNR).

Harmonic distortion and noise dictate the dynamic range of a system [12]. Over the past decade, significant effort has been made to optimize filters in terms of their dynamic range and power dissipation [13]. Companding and dynamic scaling have been proposed to optimize the dynamic range [14]. Several other techniques have been discovered to reduce the nonlinearity in transconductors and therefore in filters [1], [15]–[18].

To advance further, it is important to have an efficient tool to estimate the harmonic distortion of the filters during the design process. Most of the existing techniques use the Volterra series approach [19]–[21], where the nonlinear system is decomposed into an infinite number of subsystems with polynomial nonlinearities. Harmonic components are then evaluated separately for each subsystem. Other frequency domain methods, such as the harmonic balance method, solve the determining equations derived from balancing the harmonics, or use partial transfer functions from the input to internal nodes of the filter [13], [22].

Some of these techniques, such as those in [21] and [22], can produce analytical results of distortions in low-order weakly nonlinear systems (filters)[1] and provide some insight into the dependence of the distortion on component values. For higher order systems, especially those without a special topology, deriving closed-form analytical results using a Volterra series based approach is usually complicated with high computational costs, if possible at all.

In contrast to the widely followed path of using transfer functions or Volterra series based methods, this paper proposes a *state space* methodology for modeling and estimation of harmonic distortion. The system is described by differential equations in the time domain and all the calculations are carried out in the time domain. Although we only discuss in this paper the case of fully balanced transconductors with weak third-order

Manuscript received November 4, 2004; revised March 25, 2005. This paper was recommended by Associate Editor B. Maundy.

The authors are with the Department of Electrical and Computer Engineering, The Johns Hopkins University, Baltimore, MD 21218 USA (e-mail: zz@jhu.edu; acelik@jhu.edu; pps@jhu.edu).

Digital Object Identifier 10.1109/TCSI.2005.854296

[1]In this paper, we use the terms systems and filters interchangeably.

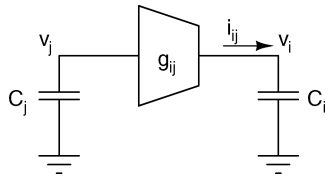

Fig. 1. A single-ended transconductor connected between node j and node i in a typical G_m-C filter.

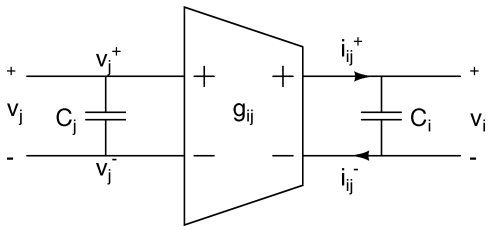

Fig. 2. Fully balanced transconductor connected between node j and node i in a typical G_m-C filter.

nonlinearity due to the simpler algebraic results, this approach can be applied to any G_m-C filters.

The paper is organized as follows. Section II introduces the notations and our assumptions, and discusses state space representation of G_m-C filters with transconductors having weak third-order nonlinearity.

In Section III, the filter is divided into the input stage, the filter core and the output stage. The distortion introduced by each stage is derived and the THD is shown to be approximately equal to the sum of the distortion introduced by each stage.

The mathematical results are compared to Cadence simulation results in Section IV for the cases of a lossy integrator and a third-order Butterworth low-pass filter.

II. G_m-C Filters With Weak Third-Order Nonlinearity and Their State Space Representation

In most practical cases, the basic building block of a G_m-C filter consists of a transconductor and a grounded capacitor. Fig. 1 shows a single-ended transconductor connected from node j to node i in a typical G_m-C filter block. If $g_{i,j}$ is its transconductance, v_j is the voltage at node j and $i_{i,j}$ is the current flowing into node i due to $g_{i,j}$, ideally we have

$$i_{i,j} = g_{i,j} v_j. \tag{1}$$

Fully differential (fully balanced) transconductors (e.g., Fig. 13) are preferred in most G_m-C filter designs, because their symmetry results in lower nonlinearity. For an ideal fully differential transconductor, Fig. 2, the equivalent of (1) is

$$i_{i,j} = g_{i,j}\left(v_j^+ - v_j^-\right) = g_{i,j} v_j.$$

Although in this paper we study G_m-C filters based on fully balanced transconductors, we use the symbol in Fig. 1 due to its simplicity.

Because of the balanced structure of the transconductor, the output current $i_{i,j}$ can be expressed using only *odd* powers of the input voltage v_j, where the fifth- and higher order terms are negligible compared to the third-order term in most practical cases, i.e.,

$$\begin{aligned} i_{i,j} &= g_{i,j} v_j + h_{i,j} v_j^3 + k_{i,j} v_j^5 + \cdots \\ &\approx g_{i,j} v_j + h_{i,j} v_j^3. \end{aligned} \tag{2}$$

These assumptions are typical in analyzing the distortion of filters with fully balanced transconductors [12], [13], [20] and are adopted here as well. Also, in many cases, the coefficient of the third-order power h_{ij} is proportional to g_{ij}, i.e.,

$$h_{ij} = \varepsilon g_{ij}.$$

The (small) constant ε has units of Volt^{-2} and can be derived analytically (see Appendix I) or extracted from the I–V characteristic of the transconductor by numerically fitting the third-order polynomial in (2) to the data from simulations or measurements (see examples in Section IV).

Although $h_{i,j} = \varepsilon g_{i,j}$ may not necessarily be true for the more general case [see (14)], it results in simpler algebraic expressions and is assumed for notational convenience (see also Appendix I). Therefore, current $i_{i,j}$ is expressed as

$$i_{i,j} = g_{i,j} v_j + \varepsilon g_{i,j} v_j^3. \tag{3}$$

Modeling G_m-C filters in state space equations is a straightforward procedure as demonstrated in the following two examples.

Example 2.1: A G_m-C lossy integrator is shown in Fig. 3 [23], [24]. The corresponding differential equation is

$$C\dot{y} = g_2 y + g_1 u. \tag{4}$$

By setting $A = g_2/C$ and $B = g_1/C$, (4) is expressed in the standard systematic form

$$\dot{y} = Ay + Bu. \tag{5}$$

Now suppose that the transconductors exhibit weak third-order nonlinearity modeled by (3). Equations (4) and (5) become, respectively

$$C\dot{y} = g_2 y + \varepsilon g_2 y^3 + g_1 u + \varepsilon g_1 u^3 \tag{6}$$

$$\dot{y} = Ay + \varepsilon A y^3 + Bu + \varepsilon B u^3. \tag{7}$$

It should be noted that the output of the filter in this example is also the state variable of the filter since it is the voltage across the capacitor. No *output transconductors* are needed in this case,

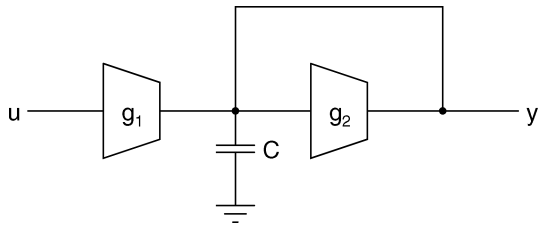

Fig. 3. A lossy G_m-C integrator.

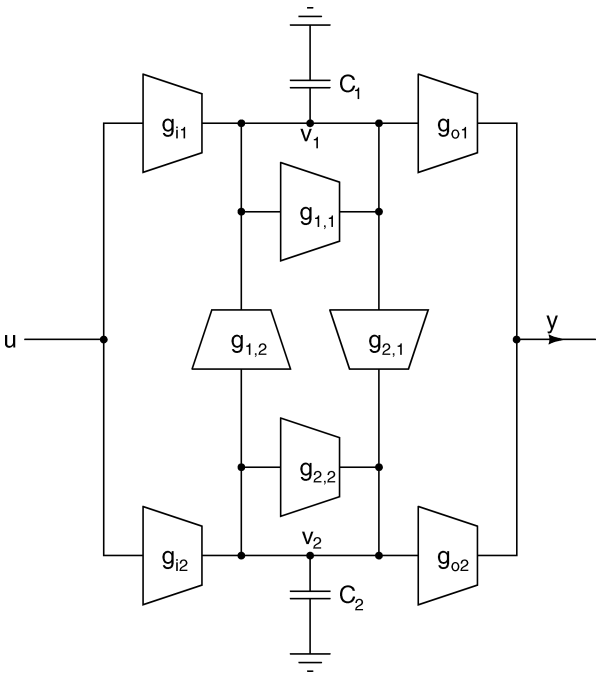

Fig. 4. A general second-order G_m-C filter with a current output.

therefore, no distortion is introduced at the *output* of the filter. This is true in many filter designs.

Example 2.2: A general form of a second-order G_m-C filter is shown in Fig. 4. If the voltages across capacitors C_1 and C_2 are v_1 and v_2, respectively, we have

$$\begin{aligned} C_1\dot{v}_1 &= g_{1,1}v_1 + g_{1,2}v_2 + g_{i1}u \\ C_2\dot{v}_2 &= g_{2,1}v_1 + g_{2,2}v_2 + g_{i2}u \\ y &= g_{o1}v_1 + g_{o2}v_2. \end{aligned} \tag{8}$$

Contrary to the previous example, the output of this filter is a current provided by the output transconductors g_{o1} and g_{o2}. If these transconductors have nonlinearities they may contribute to the total distortion of the filter.

Now if we set $\mathbf{v} = (v_1, v_2)^T$, $\dot{\mathbf{v}} = (\dot{v}_1, \dot{v}_2)^T$

$$\mathbf{A} = \begin{bmatrix} \frac{g_{1,1}}{C_1} & \frac{g_{1,2}}{C_1} \\ \frac{g_{2,1}}{C_2} & \frac{g_{2,2}}{C_2} \end{bmatrix}, \quad \mathbf{B} = \begin{bmatrix} \frac{g_{i1}}{C_1} \\ \frac{g_{i2}}{C_2} \end{bmatrix}, \quad \text{and} \quad \mathbf{C} = [g_{o1} \quad g_{o2}]$$

then (8) can be rewritten as

$$\begin{aligned} \dot{\mathbf{v}} &= \mathbf{A}\mathbf{v} + \mathbf{B}u \\ y &= \mathbf{C}\mathbf{v}. \end{aligned} \tag{9}$$

Further, if the nonlinearity of the transconductors is taken into account and modeled by (3), the filter equations become

$$\begin{aligned} C_1\dot{v}_1 &= g_{1,1}v_1 + g_{1,2}v_2 + g_{i1}u + \varepsilon\left(g_{1,1}v_1^3 + g_{1,2}v_2^3 + g_{i1}u^3\right) \\ C_2\dot{v}_2 &= g_{2,1}v_1 + g_{2,2}v_2 + g_{i2}u + \varepsilon\left(g_{2,1}v_1^3 + g_{2,2}v_2^3 + g_{i2}u^3\right) \\ y &= g_{o1}v_1 + g_{o2}v_2 + \varepsilon\left(g_{o1}v_1^3 + g_{o2}v_2^3\right). \end{aligned} \tag{10}$$

Equation (10) can be written in the matrix form

$$\begin{aligned} \dot{\mathbf{v}} &= \mathbf{A}\mathbf{v} + \mathbf{B}u + \varepsilon\mathbf{A}\mathbf{v}^{\bullet(\mathbf{3})} + \varepsilon\mathbf{B}u^3 \\ y &= \mathbf{C}\mathbf{v} + \varepsilon\mathbf{C}\mathbf{v}^{\bullet(\mathbf{3})} \end{aligned} \tag{11}$$

where $\mathbf{v}^{\bullet(3)} = (v_1^3, v_2^3, \ldots, v_n^3)^T$ is the Hadamard cube[2] of $\mathbf{v}$.

Equation (9) is the state space representation of the second-order G_m-C filter in Fig. 4 with all transconductors being linear, and (11) is the state space representation of the filter when the weak third-order nonlinearity of the transconductors is taken into account. The voltages across the capacitors, v_1 and v_2, are the *state variables*.

A general nth-order (linear) G_m-C filter can be written as a single-input, single-output nth-order linear system. Let u be the input voltage y be the output current of the filter, and let the state vector $\mathbf{v} = (v_1, v_2, \ldots, v_n)^T$ be the voltages across the capacitors. Then, the state space equations [25] of the filter are

$$\begin{aligned} \dot{\mathbf{v}} &= \mathbf{A}\mathbf{v} + \mathbf{B}u \\ y &= \mathbf{C}\mathbf{v} \end{aligned} \tag{12}$$

where $\mathbf{A} = [g_{i,j}/C_i]_{i,j=1}^n$ is the system matrix, $\mathbf{B} = [g_i/C_i]_{i=1}^n$ is the input (column) vector, g_i is the transconductor from the input to the ith capacitor C_i, and $\mathbf{C} = [c_j]_{j=1}^n$ is the output (row) vector of the system. In some cases, a *feedforward* matrix $\mathbf{D}$ may be present, i.e., $y = \mathbf{C}\mathbf{v} + \mathbf{D}u$. Since $\mathbf{D}$ simply replicates the input we can ignore it without loss of generality.

When the transconductors exhibit weak third-order nonlinearity modeled by (3), (12) changes to

$$\begin{aligned} \dot{\mathbf{v}} &= \mathbf{A}\mathbf{v} + \mathbf{B}u + \varepsilon\mathbf{A}\mathbf{v}^{\bullet(\mathbf{3})} + \varepsilon\mathbf{B}u^3 \\ y &= \mathbf{C}\mathbf{v} + \varepsilon\mathbf{C}\mathbf{v}^{\bullet(\mathbf{3})}. \end{aligned} \tag{13}$$

Equations (13) are the filter's model used in this work[3].

Throughout the paper, we assume that the linear system in (12) is asymptotically stable, the input to the filter is $u = a\sin(\omega t)$ and we use symbols in bold faces, e.g., $\mathbf{v}$ and $\mathbf{A}$, to denote vectors or matrices.

III. Estimation of Harmonic Distortion

The block diagram of the weakly nonlinear system in (13) is shown in Fig. 5. The system can be viewed as a *cascade* of three stages, the *input* stage, the *filter core* stage and the *output* stage.

[2]If $\mathbf{a} = (a_1, a_2, \ldots, a_n)^T$ and $\mathbf{b} = (b_1, b_2, \ldots, b_n)^T$ are two n-dimensional column vectors, then $\mathbf{a} \bullet \mathbf{b} = (a_1b_1, a_2b_2, \ldots, a_nb_n)^T$ is defined as the *Hadamard product* of the two vectors.

[3]If $h_{i,j} = \varepsilon g_{i,j}$ does not hold in (2), then (13) must be replaced by the more general model

$$\begin{aligned} \dot{\mathbf{v}} &= \mathbf{A}\mathbf{v} + \mathbf{E}\mathbf{v}^{\bullet(\mathbf{3})} + \mathbf{B}u + \mathbf{F}u^3 \\ y &= \mathbf{C}\mathbf{v} + \mathbf{K}\mathbf{v}^{\bullet(\mathbf{3})} \end{aligned} \tag{14}$$

where $\mathbf{E}$, $\mathbf{F}$, and $\mathbf{K}$ are the corresponding matrices for the third-order nonlinear terms. Although the algebra is a little more involved in this case, one can follow exactly the same steps presented in this paper to derive the total distortion of the filter (system).

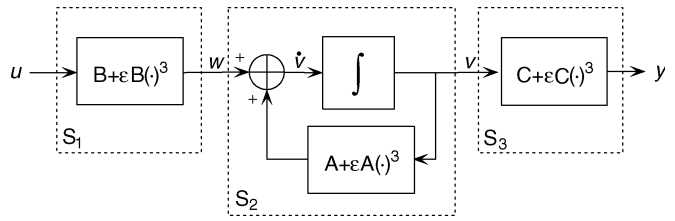

Fig. 5. Block diagram of the weakly nonlinear system in (13) viewed as a cascade of the input stage, the filter core and the output stage. The stages correspond to signal operators S_1, S_2, and S_3, respectively.

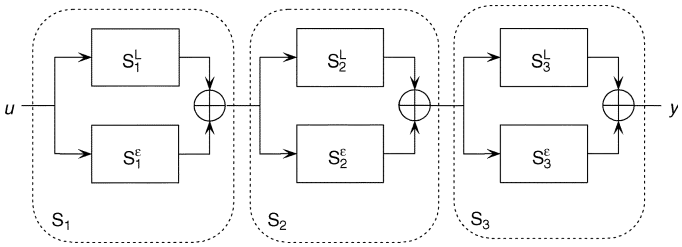

Fig. 6. Operator S_i, $i = 1, 2, 3$, is the superposition of a linear operator S_i^L and a nonlinear operator S_i^ε.

We think of these three stages as operators S_1, S_2, and S_3 in the signal space[4] such that

$$\begin{aligned} \mathbf{w} &= S_1(u) \\ \mathbf{v} &= S_2(\mathbf{w}) \\ y &= S_3(\mathbf{v}). \end{aligned} \tag{15}$$

The response of the whole system is given by the composition of operators $S_3 \circ S_2 \circ S_1$, and $y = (S_3 \circ S_2 \circ S_1)(u) = (S_3(S_2(S_1(u))))$. Each operator $S_i, i = 1, 2, 3$, can be expressed as the superposition of two operators S_i^L and S_i^ε, respectively, (see Fig. 6)

$$S_i = S_i^L + S_i^\varepsilon, \quad \text{for } i = 1, 2, \text{ and } 3. \tag{16}$$

S_i^L is the input-output relationship of the ith stage when there is no distortion (i.e., $\varepsilon = 0$), whereas the difference $S_i^\varepsilon \triangleq S_i - S_i^L$ accounts for the distortion introduced by the ith stage. It is straightforward to express the linear and nonlinear components of operators S_1 and S_3 as

$$\begin{aligned} S_1^L(u) &= \mathbf{B}u \\ S_1^\varepsilon(u) &= \varepsilon \mathbf{B}u^3 \\ S_3^L(\mathbf{v}) &= \mathbf{C}\mathbf{v} \\ S_3^\varepsilon(\mathbf{v}) &= \varepsilon \mathbf{C}\mathbf{v}^{\bullet(3)}. \end{aligned}$$

$S_2^L(\mathbf{w}) = \mathbf{v_0}$ is the *steady-state* solution of the linear system $\dot{\mathbf{v}}_\mathbf{0} = \mathbf{A}\mathbf{v}_0 + \mathbf{w}$ (see Fig. 7). $S_2^\varepsilon(\mathbf{w}) = \mathbf{v} - \mathbf{v}_0$ is the difference between the *steady-state* solutions of the systems $\dot{\mathbf{v}} = \mathbf{A}\mathbf{v} + \varepsilon\mathbf{A}\mathbf{v}^{\bullet(3)} + \mathbf{w}$ and $\dot{\mathbf{v}}_0 = \mathbf{A}\mathbf{v_0} + \mathbf{w}$, and accounts for the distortion introduced by the filter core.

[4]Note that we consider only the steady-state response of the stages in the case of a sinusoidal input u. It can been shown that for relatively small ε, signals w, v and y will also be periodic of the same period with u.

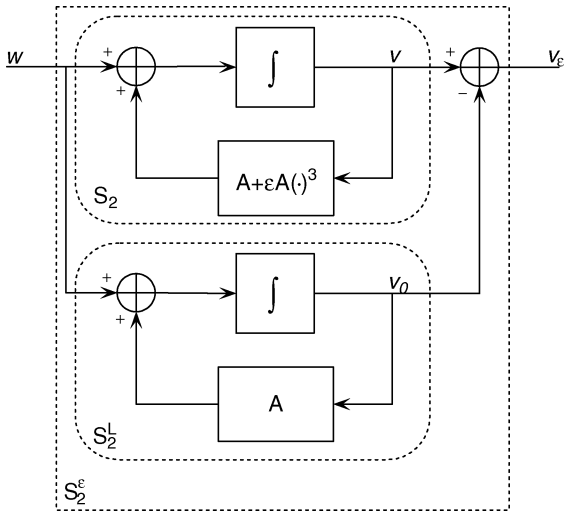

Fig. 7. Definition of operator S_2^ε.

$$\begin{aligned}
&\text{Path 1:} && u \to S_1^L \to S_2^L \to S_3^L \to y_{LLL} \\
&\text{Path 2:} && u \to S_1^\varepsilon \to S_2^L \to S_3^L \to y_{LL\varepsilon} \\
&\text{Path 3:} && u \to S_1^L \to S_2^\varepsilon \to S_3^L \to y_{L\varepsilon L} \\
&\text{Path 4:} && u \to S_1^L \to S_2^L \to S_3^\varepsilon \to y_{\varepsilon LL} \\
&\text{Path 5:} && u \to S_1^\varepsilon \to S_2^\varepsilon \to S_3^L \to y_{L\varepsilon\varepsilon} \\
&\text{Path 6:} && u \to S_1^\varepsilon \to S_2^L \to S_3^\varepsilon \to y_{\varepsilon L\varepsilon} \\
&\text{Path 7:} && u \to S_1^L \to S_2^\varepsilon \to S_3^\varepsilon \to y_{\varepsilon\varepsilon L} \\
&\text{Path 8:} && u \to S_1^\varepsilon \to S_2^\varepsilon \to S_3^\varepsilon \to y_{\varepsilon\varepsilon\varepsilon}
\end{aligned}$$

$$y = y_{LLL} + y_{LL\varepsilon} + y_{L\varepsilon L} + y_{\varepsilon LL} + y_{L\varepsilon\varepsilon} + y_{\varepsilon L\varepsilon} + y_{\varepsilon\varepsilon L} + y_{\varepsilon\varepsilon\varepsilon}$$

Fig. 8. The eight signal paths of the cascade in Fig. 6 resulting from the decomposition of operators S_1, S_2, and S_3. *Path 1* corresponds to the linear system. The output of *Paths 2, 3, 4* corresepond to the distortion generation by *only* the input, filter's core, and output stages, respectively. *Paths 5, 6, 7, 8* correspond to second- and third-order distortion and can be ignored for ε sufficiently small.

Decomposition of operators S_1, S_2, and S_3 results in eight signal paths listed in Fig. 8. Since we have assumed that the transconductors have only *weak* nonlinearity, the distortion signal components $S_1^\varepsilon(u)$, $S_2^\varepsilon(\mathbf{w})$, and $S_3^\varepsilon(\mathbf{v})$ are small compared to the desired signal components $S_1^L(u)$, $S_2^L(\mathbf{w})$, and $S_3^L(\mathbf{v})$, respectively. More accurately, it can be derived from the expressions of S_1^ε, S_2^ε, and S_3^ε, that if $\mathbf{x}$ is the input to S_i, then the amplitude of the signal $S_i^\varepsilon(\mathbf{x})$ is about $\varepsilon a_\mathbf{x}^2$ times the amplitude of $S_i^L(\mathbf{x})$, where $a_\mathbf{x}$ is the amplitude of $\mathbf{x}$. Both ε and $a_\mathbf{x}$ are considered small. In other words, the output signal

$$\begin{aligned}
y &= (S_3 \circ S_2 \circ S_1)(u) \\
&= \left(\left(S_3^L + S_3^\varepsilon\right) \circ \left(S_2^L + S_2^\varepsilon\right) \circ \left(S_1^L + S_1^\varepsilon\right)\right)(u) \\
&= \left(S_3^L \circ S_2^L \circ S_1^L\right)(u) + \left(S_3^L \circ S_2^L \circ S_1^\varepsilon\right)(u) \\
&\quad + \left(S_3^L \circ S_2^\varepsilon \circ S_1^L\right)(u) + \left(S_3^\varepsilon \circ S_2^L \circ S_1^L\right)(u) \\
&\quad + \left(S_3^L \circ S_2^\varepsilon \circ S_1^\varepsilon\right)(u) + \left(S_3^\varepsilon \circ S_2^L \circ S_1^\varepsilon\right)(u) \\
&\quad + \left(S_3^\varepsilon \circ S_2^\varepsilon \circ S_1^L\right)(u) + \left(S_3^\varepsilon \circ S_2^\varepsilon \circ S_1^\varepsilon\right)(u) \\
&= y_{LLL} + y_{LL\varepsilon} + y_{L\varepsilon L} + y_{\varepsilon LL} + y_{L\varepsilon\varepsilon} + y_{\varepsilon L\varepsilon} + y_{\varepsilon\varepsilon L} + y_{\varepsilon\varepsilon\varepsilon}
\end{aligned}$$

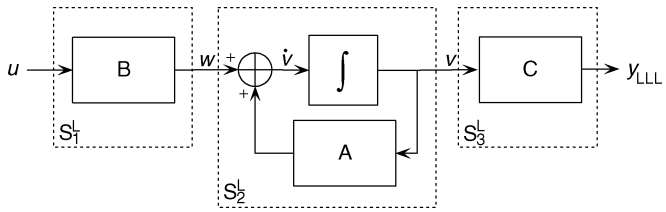

Fig. 9. Block diagram of the linear system (filter).

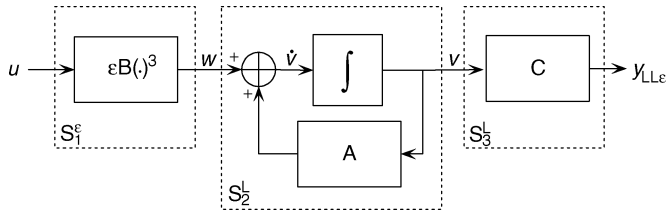

Fig. 10. Distortion introduced by the input stage when the other two stages are linear.

can be approximated by the first four terms (corresponding to *Paths* 1–4), i.e.,

$$\begin{aligned} y &\approx \left(S_3^L \circ S_2^L \circ S_1^L\right)(u) + \left(S_3^L \circ S_2^L \circ S_1^\varepsilon\right)(u) \\ &\quad + \left(S_3^L \circ S_2^\varepsilon \circ S_1^L\right)(u) + \left(S_3^\varepsilon \circ S_2^L \circ S_1^L\right)(u) \\ &= y_{LLL} + y_{LL\varepsilon} + y_{L\varepsilon L} + y_{\varepsilon LL}. \end{aligned} \tag{17}$$

In the following four subsections we derive explicit expressions for the output signals of the first four paths $(S_3^L \circ S_2^L \circ S_1^L)(u)$, $(S_3^L \circ S_2^L \circ S_1^\varepsilon)(u)$, $(S_3^L \circ S_2^\varepsilon \circ S_1^L)(u)$, and $(S_3^\varepsilon \circ S_2^L \circ S_1^L)(u)$.

A. Solution of the Linear System

Here, we consider the linear system in Fig. 9 that models the filter when $\varepsilon = 0$, i.e., all stages are linear. The problem can be described by system (18) with input $u = a\sin(\omega t)$.

$$\begin{aligned} \dot{\mathbf{v}} &= \mathbf{A}\mathbf{v} + \mathbf{B}u \\ y_{LLL} &= \mathbf{C}\mathbf{v} \end{aligned} \tag{18}$$

We use the following Lemma to derive (the steady-state response of the linear filter) $y_{LLL} = (S_3^L \circ S_2^L \circ S_1^L)(u)$. The proof can be found in Appendix II.

Lemma 3.1: If the linear system (18) is asymptotically stable and its input is $u = \alpha\cos(\omega t) + \beta\sin(\omega t)$, then its steady-state solution is $\mathbf{v} = \mathbf{p}\cos(\omega t) + \mathbf{q}\sin(\omega t)$, where $\mathbf{p}$ and $\mathbf{q}$ are column vectors given by

$$\begin{aligned} \mathbf{p} &= -(\omega^2\mathbf{I} + \mathbf{A^2})^{-1}(\alpha\mathbf{A}\mathbf{B} + \beta\omega\mathbf{B}) \\ \mathbf{q} &= -(\omega^2\mathbf{I} + \mathbf{A^2})^{-1}(\beta\mathbf{A}\mathbf{B} - \alpha\omega\mathbf{B}). \end{aligned} \tag{19}$$

Therefore, the output of the linear system in (18) is

$$\begin{aligned} y_{LLL} &= \left(S_3^L \circ S_2^L \circ S_1^L\right)(u) \\ &= -a\mathbf{C}(\omega^2\mathbf{I} + \mathbf{A^2})^{-1}\left(\omega\mathbf{B}\cos(\omega t) + \mathbf{A}\mathbf{B}\sin(\omega t)\right) \end{aligned} \tag{20}$$

B. Distortion Introduced by the Input Stage

In this section, we derive the harmonic distortion components at the output of the filter introduced by the nonlinearity of the input stage when the other two stages are linear. The situation is illustrated in Fig. 10 and corresponds to *Path* 2 in Fig. 8. The input signal is $u = a\sin(\omega t)$ as before.

To derive $y_{LL\varepsilon} = (S_3^L \circ S_2^L \circ S_1^\varepsilon)(u)$, we need to find the steady-state solution of

$$\begin{aligned} \dot{\mathbf{v}} &= \mathbf{A}\mathbf{v} + \varepsilon\mathbf{B}u^3 \\ y_{LL\varepsilon} &= \mathbf{C}\mathbf{v}. \end{aligned} \tag{21}$$

Using $\sin^3(x) = (3/4)\sin(x) - (1/4)\sin(3x)$ and applying Lemma 3.1 twice, we conclude that

$$\begin{aligned} y_{LL\varepsilon}(t) &= \left(S_3^L \circ S_2^L \circ S_1^\varepsilon\right)(u) \\ &= -\frac{3}{4}a^3\varepsilon\mathbf{C}(\omega^2\mathbf{I} + \mathbf{A^2})^{-1}(\omega\mathbf{B}\cos(\omega t) + \mathbf{A}\mathbf{B}\sin(\omega t)) \\ &\quad + \frac{1}{4}a^3\varepsilon\mathbf{C}(9\omega^2\mathbf{I} + \mathbf{A^2})^{-1} \\ &\quad \times (3\omega\mathbf{B}\cos(3\omega t) + \mathbf{A}\mathbf{B}\sin(3\omega t)). \end{aligned} \tag{22}$$

The first term in (22) is negligible because its amplitude is in general much smaller than that of the desired signal given by (20). Therefore, the distortion introduced by the nonlinearity of the input stage, when the other two stages are linear, is,

$$\mathcal{D}_1 = \frac{1}{4}a^3\varepsilon\mathbf{C}(9\omega^2\mathbf{I} + \mathbf{A^2})^{-1}\left(3\omega\mathbf{B}\cos(3\omega t) + \mathbf{A}\mathbf{B}\sin(3\omega t)\right). \tag{23}$$

Note that the amplitude of $\mathcal{D}_1$ is proportional to εa^3, i.e.,

$$\mathcal{D}_1 \propto \varepsilon a^3.$$

C. Distortion Introduced by the Filter Core

Here, we derive the harmonic distortion components introduced by the nonlinearity of the filter core when the input and output stages are linear. The setup is shown in Fig. 11 and $y_{L\varepsilon L}$ is the steady-state response of the system.

By the definition of S_2^ε (see Fig. 7), we have

$$\begin{aligned} \dot{\mathbf{v}} &= \mathbf{A}\mathbf{v} + \varepsilon\mathbf{A}\mathbf{v}^{\bullet(\mathbf{3})} + \mathbf{B}u \\ \dot{\mathbf{v}}_\mathbf{0} &= \mathbf{A}\mathbf{v}_\mathbf{0} + \mathbf{B}u \\ y_{L\varepsilon L} &= \mathbf{C}(\mathbf{v} - \mathbf{v}_\mathbf{0}). \end{aligned} \tag{24}$$

Regular perturbation theory [26] is employed to solve the nonlinear differential equations (24) (see Appendix III). The solution $\mathbf{v}$ can be found using the following procedure. First, we express $\mathbf{v}$ as an infinite series

$$\mathbf{v}(t) = \mathbf{v_0}(t) + \varepsilon\mathbf{v_1}(t) + \varepsilon^2\mathbf{v_2}(t) + \ldots.$$

Substituting into (24), we get

$$\begin{aligned} &\dot{\mathbf{v}}_\mathbf{0} + \varepsilon\dot{\mathbf{v}}_\mathbf{1} + \varepsilon^2\dot{\mathbf{v}}_\mathbf{2} + \ldots \\ &\quad = \mathbf{A}(\mathbf{v_0} + \varepsilon\mathbf{v_1} + \varepsilon^2\mathbf{v_2} + \ldots) \\ &\qquad + \varepsilon\mathbf{A}(\mathbf{v_0} + \varepsilon\mathbf{v_1} + \varepsilon^2\mathbf{v_2}\ldots)^{\bullet(3)} + \mathbf{B}u \\ &\quad = \mathbf{A}(\mathbf{v_0} + \varepsilon\mathbf{v_1} + \varepsilon^2\mathbf{v_2} + \ldots) \\ &\qquad + \varepsilon\mathbf{A}\left(\mathbf{v}_\mathbf{0}^{\bullet(3)} + 3\varepsilon\mathbf{v}_\mathbf{0}^{\bullet(2)} \bullet \mathbf{v_1} + 3\varepsilon^2\mathbf{v_0} \bullet \mathbf{v}_\mathbf{1}^{\bullet(2)} + \ldots\right) \\ &\qquad + \mathbf{B}u \end{aligned}$$

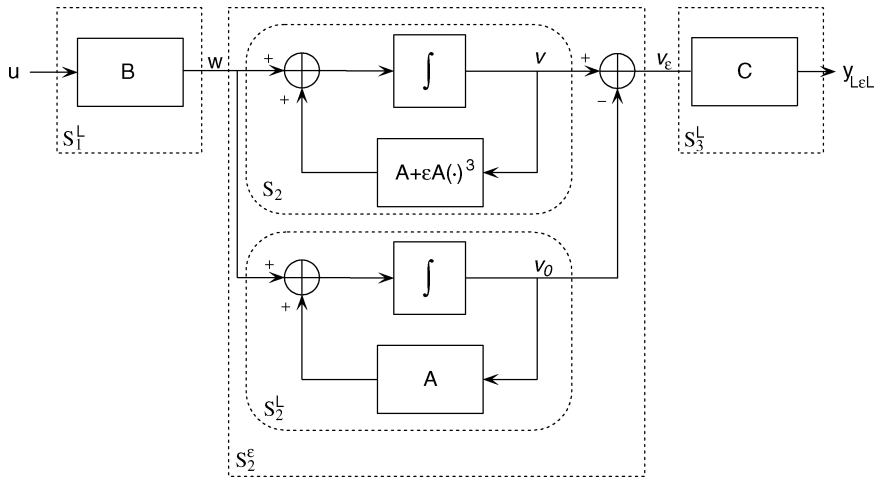

Fig. 11. Distortion introduced by the filter core when the other two stages are linear.

Next, the summands are grouped based on the power of ε

$$\dot{\mathbf{v}}_\mathbf{0}+\varepsilon\dot{\mathbf{v}}_\mathbf{1}+\varepsilon^2\dot{\mathbf{v}}_\mathbf{2}+\ldots=\mathbf{A}\mathbf{v}_\mathbf{0}+\mathbf{B}u+\varepsilon\left(\mathbf{A}\mathbf{v}_\mathbf{1}+\mathbf{A}\mathbf{v}_\mathbf{0}^{\bullet(3)}\right)+\varepsilon^2\left(\mathbf{A}\mathbf{v}_\mathbf{2}+3\mathbf{A}(\mathbf{v}_\mathbf{0}^{\bullet(2)}\bullet\mathbf{v}_\mathbf{1})\right)+\ldots.$$

Equating ε-terms of the same power yields

$$\dot{\mathbf{v}}_\mathbf{0}=\mathbf{A}\mathbf{v}_\mathbf{0}+\mathbf{B}u \tag{25}$$

$$\dot{\mathbf{v}}_\mathbf{1}=\mathbf{A}\mathbf{v}_\mathbf{1}+\mathbf{A}\mathbf{v}_\mathbf{0}^{\bullet(3)} \tag{26}$$

$$\dot{\mathbf{v}}_\mathbf{2}=\mathbf{A}\mathbf{v}_\mathbf{2}+3\mathbf{A}(\mathbf{v}_\mathbf{0}^{\bullet(2)}\bullet\mathbf{v}_\mathbf{1}).$$

$$\vdots$$

The solution of (24) can be obtained by solving this infinite set of equations. Since ε is assumed small and all the distortion components are also expected to be small relative to the desired signal, $\mathbf{v}$ can be well approximated by only the first two terms in the series, i.e., $\mathbf{v}\approx\mathbf{v_0}+\varepsilon\mathbf{v_1}$. When the input is $u=a\sin(\omega t)$, the solution for $\mathbf{v_0}$ comes directly from Lemma 3.1

$$\mathbf{v_0}=-a(\omega^2\mathbf{I}+\mathbf{A^2})^{-1}\left(\omega\mathbf{B}\cos(\omega t)+\mathbf{AB}\sin(\omega t)\right). \tag{27}$$

To solve (26), it is convenient to write $\mathbf{v_0}=\mathbf{r}\cos(\omega t)+\mathbf{s}\sin(\omega t)$ where

$$\begin{aligned}\mathbf{r}&\triangleq-a(\omega^2\mathbf{I}+\mathbf{A^2})^{-1}\omega\mathbf{B}\\ \mathbf{s}&\triangleq-a(\omega^2\mathbf{I}+\mathbf{A^2})^{-1}\mathbf{AB}.\end{aligned} \tag{28}$$

Then we have

$$\begin{aligned}\mathbf{v}_\mathbf{0}^{\bullet(3)}=&\left(\frac{3}{4}\mathbf{r}^{\bullet(3)}+\frac{3}{4}\mathbf{r}\bullet\mathbf{s}^{\bullet(2)}\right)\cos(\omega t)\\&+\left(\frac{3}{4}\mathbf{s}^{\bullet(3)}+\frac{3}{4}\mathbf{r}^{\bullet(2)}\bullet\mathbf{s}\right)\sin(\omega t)\\&+\left(\frac{1}{4}\mathbf{r}^{\bullet(3)}-\frac{3}{4}\mathbf{r}\bullet\mathbf{s}^{\bullet(2)}\right)\cos(3\omega t)\\&+\left(-\frac{1}{4}\mathbf{s}^{\bullet(3)}+\frac{3}{4}\mathbf{r}^{\bullet(2)}\bullet\mathbf{s}\right)\sin(3\omega t)\end{aligned}$$

which can be rewritten as

$$\mathbf{v}_\mathbf{0}^{\bullet(3)}=\mathbf{p_1}\cos(\omega t)+\mathbf{q_1}\sin(\omega t)+\mathbf{p_3}\cos(3\omega t)+\mathbf{q_3}\sin(3\omega t) \tag{29}$$

by setting

$$\begin{aligned}\mathbf{p_1}&=\frac{3}{4}\mathbf{r}^{\bullet(3)}+\frac{3}{4}\mathbf{r}\bullet\mathbf{s}^{\bullet(2)}\\ \mathbf{q_1}&=\frac{3}{4}\mathbf{s}^{\bullet(3)}+\frac{3}{4}\mathbf{r}^{\bullet(2)}\bullet\mathbf{s}\\ \mathbf{p_3}&=\frac{1}{4}\mathbf{r}^{\bullet(3)}-\frac{3}{4}\mathbf{r}\bullet\mathbf{s}^{\bullet(2)}\\ \mathbf{q_3}&=-\frac{1}{4}\mathbf{s}^{\bullet(3)}+\frac{3}{4}\mathbf{r}^{\bullet(2)}\bullet\mathbf{s}.\end{aligned} \tag{30}$$

Applying Lemma 3.1 and using (29) and (30), we have the solution of (26)

$$\begin{aligned}\mathbf{v_1}=&-(\omega^2\mathbf{I}+\mathbf{A^2})^{-1}\mathbf{A}(\mathbf{Ap_1}+\omega\mathbf{q_1})\cos(\omega t)\\&-(\omega^2\mathbf{I}+\mathbf{A^2})^{-1}\mathbf{A}(\mathbf{Aq_1}-\omega\mathbf{p_1})\sin(\omega t)\\&-(9\omega^2\mathbf{I}+\mathbf{A^2})^{-1}\mathbf{A}(\mathbf{Ap_3}+3\omega\mathbf{q_3})\cos(3\omega t)\\&-(9\omega^2\mathbf{I}+\mathbf{A^2})^{-1}\mathbf{A}(\mathbf{Aq_3}-3\omega\mathbf{p_3})\sin(3\omega t)\end{aligned} \tag{31}$$

Equation (24) along with approximation $\mathbf{v}\approx\mathbf{v_0}+\varepsilon\mathbf{v_1}$ implies

$$\begin{aligned}y_{L\varepsilon L}=&\left(S_3^L\circ S_2^\varepsilon\circ S_1^L\right)(u)\approx\mathbf{C}\varepsilon\mathbf{v_1}\\&-\varepsilon\mathbf{C}(\omega^2\mathbf{I}+\mathbf{A^2})^{-1}\mathbf{A}(\mathbf{Ap_1}+\omega\mathbf{q_1})\cos(\omega t)\\&-\varepsilon\mathbf{C}(\omega^2\mathbf{I}+\mathbf{A^2})^{-1}\mathbf{A}(\mathbf{Aq_1}-\omega\mathbf{p_1})\sin(\omega t)\\&-\varepsilon\mathbf{C}(9\omega^2\mathbf{I}+\mathbf{A^2})^{-1}\mathbf{A}(\mathbf{Ap_3}+3\omega\mathbf{q_3})\cos(3\omega t)\\&-\varepsilon\mathbf{C}(9\omega^2\mathbf{I}+\mathbf{A^2})^{-1}\mathbf{A}(\mathbf{Aq_3}-3\omega\mathbf{p_3})\sin(3\omega t)\end{aligned} \tag{32}$$

The signal components in $y_{L\varepsilon L}$ at frequency ω are negligible compared to the desired signal given by (20). The distortion introduced by the filter core is[5]

$$\begin{aligned}\mathcal{D}_2\approx-\varepsilon\mathbf{C}(9\omega^2\mathbf{I}+\mathbf{A^2})^{-1}\mathbf{A}\,&((\mathbf{Ap_3}+3\omega\mathbf{q_3})\cos(3\omega t)\\&+(\mathbf{Aq_3}-3\omega\mathbf{p_3})\sin(3\omega t))\end{aligned} \tag{33}$$

Note that $\mathbf{r},\mathbf{s}$ are proportional to the amplitude a, which implies that $\mathbf{p_1}$, $\mathbf{q_1}$, $\mathbf{p_3}$, $\mathbf{q_3}$ are all proportional to a^3 and therefore

$$\mathcal{D}_2\propto\varepsilon a^3.$$

[5]Higher order harmonics may be present at the output of the filter, though they are negligible compared to the third-order harmonic, which dominates the distortion of the output. $(S_3^L\circ S_2^\varepsilon\circ S_1^L)(u)$ contains only third-order harmonic because of the approximation $\mathbf{v}\approx\mathbf{v_0}+\varepsilon\mathbf{v_1}$.

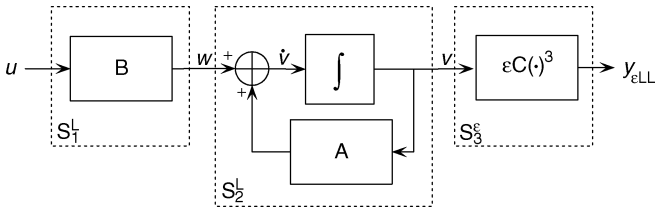

Fig. 12. Distortion introduced by the output stage when the other two stages are linear.

D. Distortion Introduced by Output Stage

Here, we derive the harmonic distortion introduced by the output stage when the input stage and the filter core are linear. Fig. 12 illustrates the setup and the corresponding dynamical system is given by (34). The input signal is $u(t) = a\sin(\omega t)$ and $y_{\varepsilon LL}$ is the steady-state response of the system.

$$\begin{aligned}\dot{\mathbf{v}} &= \mathbf{A}\mathbf{v} + \mathbf{B}u \\ y_{\varepsilon LL} &= \varepsilon \mathbf{C}\mathbf{v}^{\bullet(\mathbf{3})}\end{aligned} \tag{34}$$

$\mathbf{v}$ in (34) has been derived and is given by (27). Using (29), we have

$$\mathbf{v}^{\bullet(3)} = \mathbf{p_1}\cos(\omega t) + \mathbf{q_1}\sin(\omega t) + \mathbf{p_3}\cos(3\omega t) + \mathbf{q_3}\sin(3\omega t) \tag{35}$$

and

$$\begin{aligned} y_{\varepsilon LL} &= \varepsilon \mathbf{C}\mathbf{v}^{\bullet(\mathbf{3})} \\ &= \varepsilon \mathbf{C}\Big(\mathbf{p_1}\cos(\omega t) + \mathbf{q_1}\sin(\omega t) \\ &\qquad + \mathbf{p_3}\cos(3\omega t) + \mathbf{q_3}\sin(3\omega t)\Big). \end{aligned} \tag{36}$$

Again, the signal components of $y_{\varepsilon LL}$ at frequency ω are negligible, hence the distortion introduced by the nonlinearity of the output stage, when the other two stages are linear, is

$$\mathcal{D}_3 = \varepsilon \mathbf{C}\left(\mathbf{p_3}\cos(3\omega t) + \mathbf{q_3}\sin(3\omega t)\right). \tag{37}$$

Since $\mathbf{p_3}$, $\mathbf{q_3}$ are proportional to a^3 [see (30) and (28)], we have

$$\mathcal{D}_3 \propto \varepsilon a^3.$$

E. Total Harmonic Distortion

The total third-order harmonic components at the output of the filter are

$$\begin{aligned} \mathcal{D}_1 + \mathcal{D}_2 + \mathcal{D}_3 &= \left(S_3^L \circ S_2^L \circ S_1^\varepsilon\right)(u) \\ &\quad + \left(S_3^L \circ S_2^\varepsilon \circ S_1^L\right)(u) \\ &\quad + \left(S_3^\varepsilon \circ S_2^L \circ S_1^L\right)(u) \\ &= y_{LL\varepsilon} + y_{L\varepsilon L} + y_{\varepsilon LL} \\ &= D_c\cos(3\omega t) + D_s\sin(3\omega t) \end{aligned}$$

where

$$\begin{aligned} D_c = &\underbrace{\frac{3}{4}a^3\varepsilon\omega\mathbf{C}(9\omega^2\mathbf{I} + \mathbf{A^2})^{-1}\mathbf{B}}_{\text{input}} \\ &\underbrace{-\varepsilon\mathbf{C}(9\omega^2\mathbf{I} + \mathbf{A^2})^{-1}(\mathbf{A^2 p_3} + 3\omega\mathbf{A q_3})}_{\text{filtercore}} + \underbrace{\varepsilon\mathbf{C p_3}}_{\text{output}} \\ D_s = &\underbrace{\frac{1}{4}a^3\varepsilon\mathbf{C}(9\omega^2\mathbf{I} + \mathbf{A^2})^{-1}\mathbf{A}\mathbf{B}}_{\text{input}} \\ &\underbrace{-\varepsilon\mathbf{C}(9\omega^2\mathbf{I} + \mathbf{A^2})^{-1}(\mathbf{A^2 q_3} - 3\omega\mathbf{A p_3})}_{\text{filtercore}} + \underbrace{\varepsilon\mathbf{C q_3}}_{\text{output}} \end{aligned}$$

and both D_c and D_s are proportional to εa^3.

Remark: The expressions of D_c and D_s were derived assuming that ALL three stages of the filter are nonlinear and contribute to the total distortion of the filter. If any of them is linear or is not present (see Example 2.1) the corresponding terms in D_c and D_s should be removed.

The desired signal at the output of the filter is approximated by the linear filter output

$$\begin{aligned} y_{LLL} &= -a\mathbf{C}(\omega^2\mathbf{I} + \mathbf{A^2})^{-1}\left(\omega\mathbf{B}\cos(\omega t) + \mathbf{A}\mathbf{B}\sin(\omega t)\right) \\ &= S_c\cos(\omega t) + S_s\sin(\omega t) \end{aligned}$$

where

$$\begin{aligned} S_c &= -a\omega\mathbf{C}(\omega^2\mathbf{I} + \mathbf{A^2})^{-1}\mathbf{B} \\ S_s &= -a\mathbf{C}(\omega^2\mathbf{I} + \mathbf{A^2})^{-1}\mathbf{A}\mathbf{B}. \end{aligned}$$

The THD of a G_m-C filter modeled by (13) is

$$\text{THD} \approx 10\log_{10}\left(\frac{D_c^2 + D_s^2}{S_c^2 + S_s^2}\right) \quad \text{(dB)} \tag{38}$$

Since D_c and D_s are proportional to εa^3, and S_c and S_s are proportional to a, we get

$$\text{THD} = 20\log_{10}(|\varepsilon|) + 40\log_{10}(a) + \Gamma(\mathbf{A}, \mathbf{B}, \mathbf{C}, \omega) \tag{39}$$

where Γ is a function of only the system parameters and frequency ω. If $|\varepsilon|$ is reduced to $|\varepsilon|/10$, the power of the third-order harmonic distortion and the THD will both drop by 20 dB. If a is reduced to $a/10$, the power of the third-order harmonic distortion and the THD will be attenuated by 60 dB and 40 dB, respectively.

Note that these results apply to nonlinear systems without memory as well. Consider for example a single transconductor with weak third-order nonlinearity, $i_o = gu + \varepsilon g u^3$, and input signal $u(t) = a\sin(\omega t)$. The harmonic components at the output consist of a third-order term of amplitude $(1/4)|\varepsilon| g a^3$. The amplitude of the desired signal is ga, and so THD $\approx 20\log_{10}((1/4)|\varepsilon|a^2) = 20\log_{10}(|\varepsilon|) + 40\log_{10}(a) - 20\log_{10}(4)$.

The proposed process to derive the THD is summarized in Appendix IV and can be easily implemented in MATLAB.

IV. Simulations

The proposed THD derivation process is verified in Cadence SpectreS simulator using the lossy integrator in Fig. 3 and a third-order low-pass filter. In our simulations, we use the typical

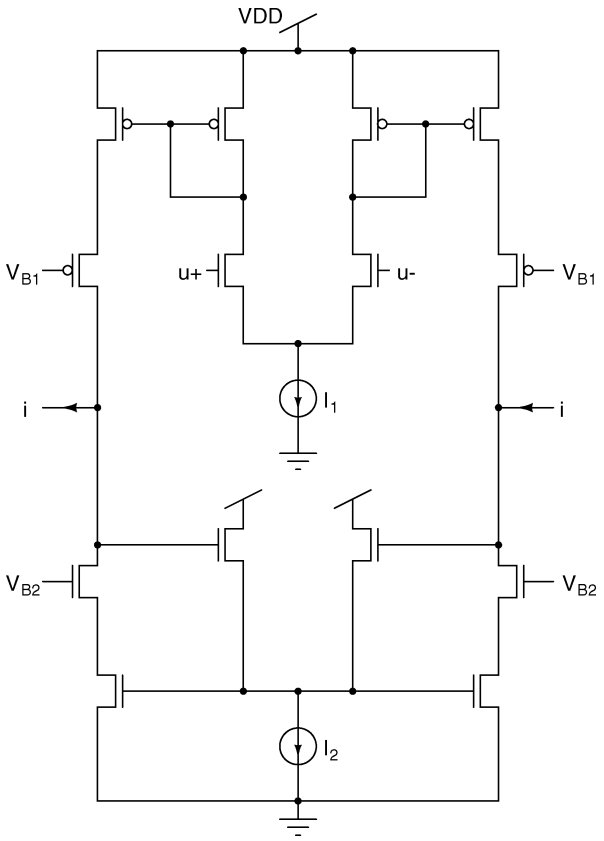

Fig. 13. Schematic of the transconductor used in Cadence SpectreS simulation of the lossy integrator and the third-order Butterworth low-pass filter.

fully balanced, cascode-output transconductor in Fig. 13 with transistor models for the AMI 0.5-μm process (AMIS C5).

In these simulations, the filters are driven by a sinusoidal input signal and a transient analysis is performed. The filter outputs are passed on to the FFT function to calculate the THD.

To find the linear transconductance g and the ε parameter, a dc sweep analysis is performed on the transconductor and the response is plotted in Fig. 14. This *I-V* characteristic is then exported to MATLAB for curve fitting using a third-order polynomial. We get $g = 5.384 \times 10^{-5}\ \Omega^{-1}$ and $\varepsilon = -0.229\ \mathrm{V}^{-2}$. These values are used in our MATLAB implementation of the proposed algorithm (summarized in Appendix IV) to estimate the THD. The results are compared to those from SpectreS simulations and reported in details in the following.

A. Lossy Integrator: Revisited

If we assume that $C = 2$ pF in Fig. 3, by following example 2.1, we have $A = B = g/C = 2.692 \times 10^7\ \mathrm{s}^{-1}$. The amplitude of the sinusoidal input is $a = 0.1$ V.

The THD values from SpectreS simulations and MATLAB implementations are plotted in Fig. 15. The simulation and theoretical results are in good agreement especially when the frequency of the input signal is below the 3-dB bandwidth, $f_{-3dB} = g/(2\pi C) = 4.285$ MHz, of the integrator. A major part of the error is due to the bandwidth limitations of the

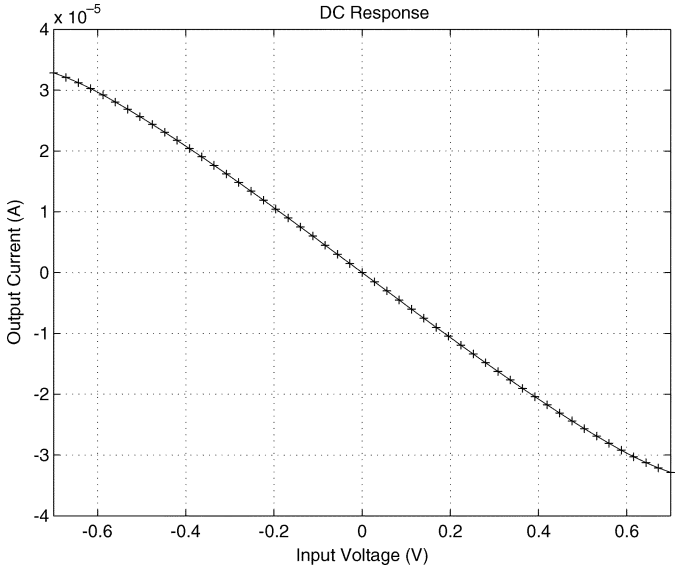

Fig. 14. DC response of the transconductor in Fig. 13.

transconductors and the phase errors they introduce, hence the mismatch between the circuit and the derived systematic model.

To further support the discussion in Section III-C, a fast Fourier transform (FFT) is performed on the filter output signal, and the result is shown in Fig. 16. For the given input, the fifth-order harmonic is about 40 dB below the third-order harmonic and harmonics of even higher order are practically undetectable.

B. Third-Order Low-Pass Filter

The second test filter is shown in Fig. 17. It is a *third-order Butterworth low-pass* filter with transfer function

$$H(s) = \frac{Y(s)}{U(s)} = \frac{1}{\left(\frac{s}{\omega_0}+1\right)\left(\left(\frac{s}{\omega_0}\right)^2 + \left(\frac{s}{\omega_0}\right) + 1\right)} \tag{40}$$

and 3-dB frequency $f_0 = (\omega_0/2\pi) = (g/2\pi C) = 1.07$ MHz. As before, we have $g = 5.384 \times 10^{-5}\ \Omega^{-1}$ and $\varepsilon = -0.229\ \mathrm{V}^{-2}$. In this example, $C = 8$ pF. Let v_1, v_2 and v_3 be the node voltages as shown in Fig. 17 it is then for the linear (ideal) filter we have

$$\begin{aligned} \dot{v}_1 &= -\frac{g}{C}v_1 + \frac{g}{C}u \\ \dot{v}_2 &= \frac{g}{C}v_1 - \frac{g}{C}v_2 - \frac{g}{C}v_3 \\ \dot{v}_3 &= \frac{g}{C}v_2 \\ y &= v_3 \end{aligned} \tag{41}$$

which can be written in the standard form

$$\begin{aligned} \dot{\mathbf{v}} &= \mathbf{A}\mathbf{v} + \mathbf{B}u \\ y &= \mathbf{C}\mathbf{v} \end{aligned} \tag{42}$$

where $\mathbf{v} = [v_1, v_2 v_3]^T$, $\dot{\mathbf{v}} = [\dot{v}_1, \dot{v}_2, \dot{v}_3]^T$

$$\mathbf{A} = \begin{bmatrix} -\frac{g}{C} & 0 & 0 \\ \frac{g}{C} & -\frac{g}{C} & -\frac{g}{C} \\ 0 & \frac{g}{C} & 0 \end{bmatrix},\ \mathbf{B} = \begin{bmatrix} \frac{g}{C} \\ 0 \\ 0 \end{bmatrix},\ \text{and}\ \mathbf{C} = [0\ 0\ 1].$$

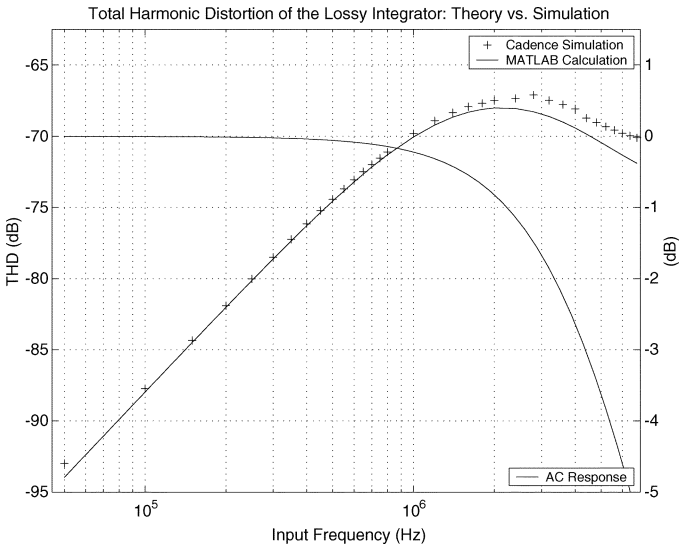

Fig. 15. Cadence SpectreS simulation and MATLAB calculation of the THD at the output of the lossy integrator in Fig. 3. The distortion is plotted against the y axis on the left, while the frequency response of the lossy integrator is measured against the y axis on the right.

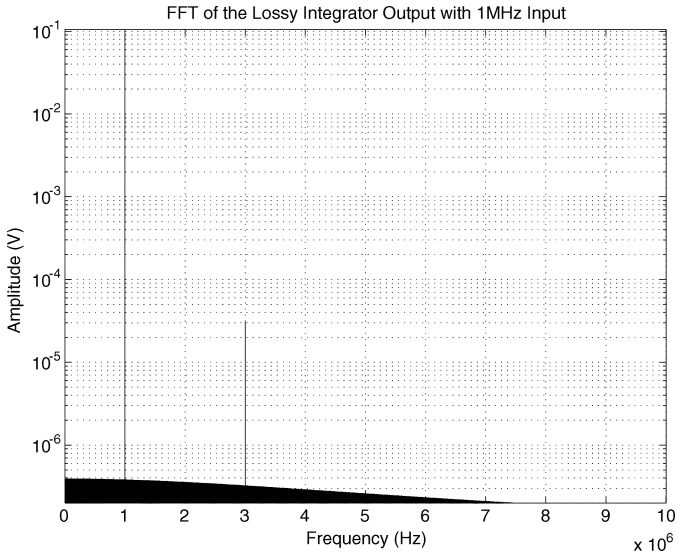

Fig. 16. FFT of Cadence simulation output of the lossy integrator in Fig. 3 with 1 MHz, 0.1 V sinusoidal input, and 2 pF capacitance. Only odd-order harmonics (3 MHz, 5 MHz. . .) are present.

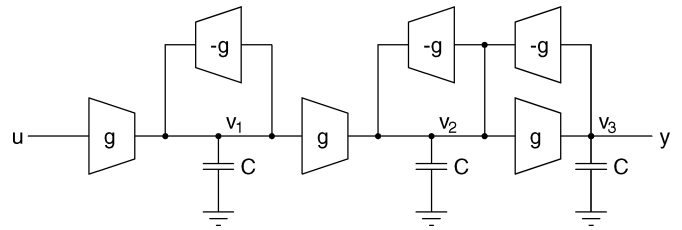

Fig. 17. Third-order Butterworth low-pass G_m-C filter.

Fig. 18 shows the THD of the filter obtained from Cadence simulations and the proposed algorithm (see Appendix IV) implemented in MATLAB. We used the FFT function to extract the harmonic signals amplitudes from Cadence simulation. This is computationally expensive requiring numerical processing of thousands of signal periods after the transients of the filter have faded out. The theoretical results are in good agreement with the simulation estimates, especially when the frequency of the input signal is below the 3-dB frequency $f_0 = g/(2\pi C) = 1.07$ MHz. Also, note that the three distortion curves corresponding to input amplitudes a =0.1, 0.2, and 0.4 V are very similar in shape and *shifted vertically* relative to each other by $40\log_{10}(2) \approx 12.04$ dB as was predicted by (39).

The discrepancy between results obtained from Cadence and MATLAB is mainly due to numerical errors in the extraction of distortion from the Cadence simulation data and not due to the approximations made in the theoretical derivation. Another source contributing to the error is the limited bandwidth of the transconductors used in the simulations. The phase shift introduced by them and in general their dynamic behavior can be—to some extent—incorporated into the filter's dynamics.

V. Conclusion

The paper presents a state-space approach to estimating the THD of G_m-C filters with weakly nonlinear fully balanced transconductors. The derived algorithm is implemented in MATLAB. The results from the algorithm are compared with those from Cadence SpectreS simulations for two example filters and they are in good agreement. Major advantages of this approach is its very low numerical complexity and the fact that the resulting formulas depend directly on the component values of the filter (matrices $\mathbf{A}$, $\mathbf{B}$ and $\mathbf{C}$). This approach also applies to any arbitrary G_m-C filter. Since it is easily implementable in MATLAB, one can directly modify the structural matrices until the THD drops below the desirable levels. This allows for automated filter optimization.

Appendix I
Analytical Derivation of ε: An Example

Consider the MOSFET differential pair in Fig. 19. It can be shown [27] that the drain currents of the two MOSFETs are

$$i_{D1} = \frac{I}{2} + \sqrt{k_n' \frac{W}{L} I}\left(\frac{v_{id}}{2}\right)\sqrt{1 - \frac{\left(\frac{v_{id}}{2}\right)^2}{\frac{I}{\left(k_n' \frac{W}{L}\right)}}} \tag{43}$$

$$i_{D2} = \frac{I}{2} - \sqrt{k_n' \frac{W}{L} I}\left(\frac{v_{id}}{2}\right)\sqrt{1 - \frac{\left(\frac{v_{id}}{2}\right)^2}{\frac{I}{\left(k_n' \frac{W}{L}\right)}}} \tag{44}$$

where $k_n' = (1/2)\mu_n C_{\text{ox}}$. In most cases, the output current is proportional to the current difference

$$\begin{aligned} i_o &= \eta(i_{D1} - i_{D2}) \\ &= 2\eta\sqrt{k_n' \frac{W}{L} I}\left(\frac{v_{id}}{2}\right)\sqrt{1 - \frac{\left(\frac{v_{id}}{2}\right)^2}{\frac{I}{\left(k_n' \frac{W}{L}\right)}}} \end{aligned} \tag{45}$$

Since $\sqrt{1-(x/2)^2} = 1 - (1/8)x^2 +$ higher order terms (x), (44) gives that

$$\begin{aligned} i_o &= \left(\eta\sqrt{k_n' \frac{W}{L} I}\right) v_{id} - \frac{\eta}{8}\frac{v_{id}^3}{\frac{I}{\left(k_n' \frac{W}{L}\right)}}\sqrt{k_n' \frac{W}{L} I} \\ &\quad + \text{Higher Order Terms} \qquad (46) \\ &= g_m v_{id} + \varepsilon g_m v_{id}^3 + \text{Higher Order Terms} \qquad (47) \end{aligned}$$

where $g_m = \eta\sqrt{k_n'(W/L)I}$ and $\varepsilon = -(1/8)/(I/(k_n'(W/L)))$.

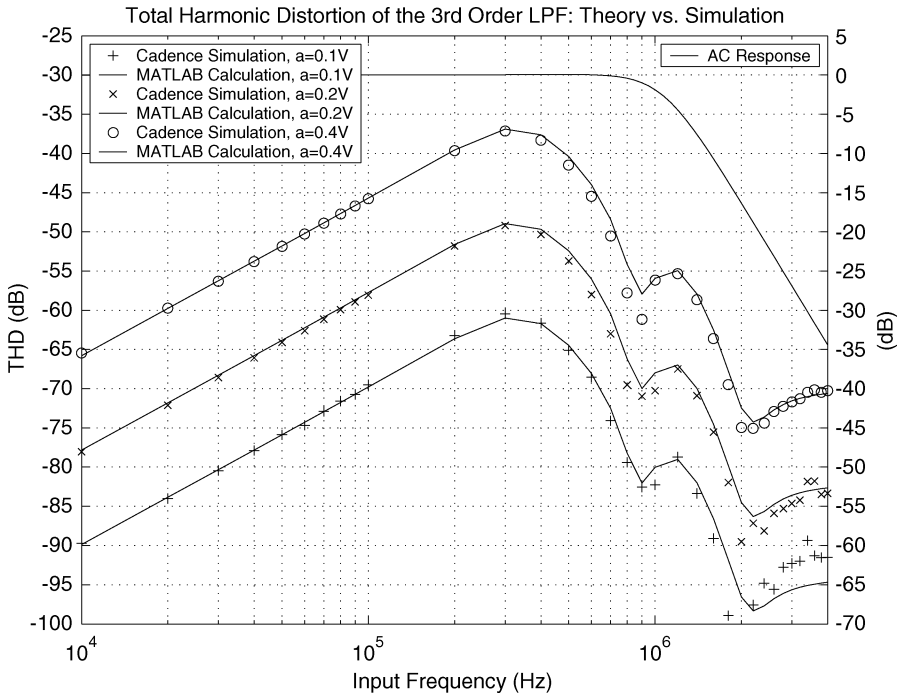

Fig. 18. THD of the third-order Butterworth low-pass filter with respect to frequency for input amplitudes a =0.1, 0.2, and 0.4 V. Results derived by using the proposed algorithm (see Appendix IV) implemented in MATLAB are plotted by solid lines, while data points from Cadence simulations are marked with "+," "x," and "o." The ac response of the filter is plotted against the y axis on the right. The error remains less than 1.7 dB with the exception of one point when the input signal frequency is below the 3-dB frequency of 1.07 MHz. At higher frequencies, well within the rejection band, the error increases but remains less than 4.5 dB. Though larger errors occur when the distortion is less than -80 dB, they are mainly introduced when harmonic signals are extracted from the simulation data and can be reduced by using an even larger set of data.

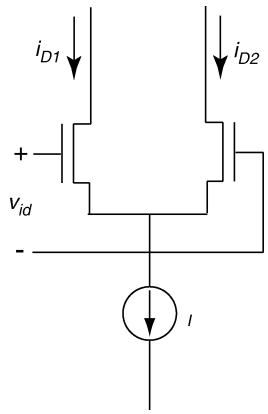

Fig. 19. A MOSFET differential pair as a basic transconductor.

Appendix II
Proof of Lemma 3.1

Since the system $\dot{\mathbf{v}} = \mathbf{A}\mathbf{v} + \mathbf{B}u$ is assumed to be asymptotically stable and the input is $u(t) = \alpha\cos(\omega t) + \beta\sin(\omega t)$, the steady-state solution must be of the same form [28], $\mathbf{v} = \mathbf{p}\cos(\omega t) + \mathbf{q}\sin(\omega t)$. To find $\mathbf{p}$ and $\mathbf{q}$, we differentiate both sides of $\dot{\mathbf{v}} = \mathbf{A}\mathbf{v} + \mathbf{B}u$ and get

$$\begin{aligned}\ddot{\mathbf{v}} &= \mathbf{A}\dot{\mathbf{v}} + \mathbf{B}\dot{u} \\ &= \mathbf{A}(\mathbf{A}\mathbf{v} + \mathbf{B}u) + \mathbf{B}\dot{u} \\ &= \mathbf{A}^2\mathbf{v} + \mathbf{A}\mathbf{B}u + \mathbf{B}\dot{u}. \end{aligned} \tag{48}$$

Substituting u and $\mathbf{v}$ into (48), we get

$$\begin{aligned}&-\omega^2\mathbf{p}\cos(\omega t) - \omega^2\mathbf{q}\sin(\omega t) = \mathbf{A}^2\left(\mathbf{p}\cos(\omega t) + \mathbf{q}\sin(\omega t)\right) \\ &+\mathbf{A}\mathbf{B}\left(\alpha\cos(\omega t) + \beta\sin(\omega t)\right) + \mathbf{B}\left(-\omega\alpha\sin(\omega t) + \omega\beta\cos(\omega t)\right)\end{aligned}$$

Separating "sin" and "cos" terms gives

$$\begin{aligned}\mathbf{p} &= -(\omega^2\mathbf{I} + \mathbf{A}^2)^{-1}(\alpha\mathbf{A}\mathbf{B} + \beta\omega\mathbf{B}) \\ \mathbf{q} &= -(\omega^2\mathbf{I} + \mathbf{A}^2)^{-1}(\beta\mathbf{A}\mathbf{B} - \alpha\omega\mathbf{B}).\end{aligned}$$

Appendix III
A Result From Perturbation Theory for Ordinary Differential Equations

Consider the system described by differential equation[6] (49) along with initial condition (50).

$$\dot{\mathbf{x}} = \mathbf{f}(t, \mathbf{x}, \epsilon) \tag{49}$$

$$\mathbf{x}(t_0) = \mathbf{x_0}. \tag{50}$$

The following theorem is borrowed from [29]. More details about (regular) perturbation theory can be found, for example, in [26], [28], and [30].

Theorem 3.1: If $\mathbf{f}$ has continuous derivatives up to order N and the problem (49), (50) has a unique solution when $\epsilon = 0$, then there exists an $\epsilon^* > 0$ such that the problem (49), (50) has a unique solution $\mathbf{x}(t, \epsilon)$ for every $|\epsilon| < \epsilon^*$. Moreover, there exist functions $\mathbf{x}_0$, $\mathbf{x}_1$, $\mathbf{x}_2 \ldots$ such that $\mathbf{x}(t, \epsilon) - \sum_{k=0}^{N-1} \mathbf{x_k}(t)\epsilon^k = O(\epsilon^N)$. The functions $\mathbf{x_k}$ can be derived by solving the systems

$$\frac{\partial^k}{\partial \epsilon^k}\left(\sum_{k=0}^{\infty} \mathbf{x_k}(t)\epsilon^k\right)_{\epsilon=0} = \frac{\partial^k}{\partial \epsilon^k}\left(\mathbf{f}\left(t, \sum_{k=0}^{\infty} \mathbf{x_k}(t)\epsilon^k, \epsilon\right)\right)_{\epsilon=0} \tag{51}$$

with $\mathbf{x}_0(t_0) = \mathbf{x_0}$ and $\mathbf{x}_k(t_0) = 0$ for all $k > 0$.

[6]Note that a system with an input u can also be treated as a time dependent system.

APPENDIX IV
STEPS TO FIND THE THD

The proposed process for deriving the THD is summarized in seven steps. The seventh step gives the distortion components explicitly.

1) *Find the state space representation* (13) *of the G_m-C filter*.

   Find matrices $\mathbf{A}$, $\mathbf{B}$ and $\mathbf{C}$ (see Examples 2.1 and 2.2). Derive ε analytically (see Appendix I) or experimentally by fitting a third-order polynomial to the $I-V$ characteristic of the transconductor (see Section IV). Choose the amplitude a and frequency ω of the input signal $u(t) = a\sin(\omega t)$.

2) *Calculate* $\mathbf{r}$ *and* $\mathbf{s}$

$$\mathbf{r} = -a(\omega^2\mathbf{I}+\mathbf{A^2})^{-1}\omega\mathbf{B}$$
$$\mathbf{s} = -a(\omega^2\mathbf{I}+\mathbf{A^2})^{-1}\mathbf{AB}.$$

3) *Calculate* $\mathbf{p_3}$, $\mathbf{q_3}$

$$\mathbf{p_3} = \frac{1}{4}\mathbf{r}^{\bullet(3)} - \frac{3}{4}\mathbf{r}\bullet\mathbf{s}^{\bullet(2)}$$
$$\mathbf{q_3} = -\frac{1}{4}\mathbf{s}^{\bullet(3)} + \frac{3}{4}\mathbf{r}^{\bullet(2)}\bullet\mathbf{s}.$$

4) *Calculate* $\mathbf{S_c}$ *and* $\mathbf{S_s}$

$$S_c = \mathbf{Cr}$$
$$S_s = \mathbf{Cs}.$$

5) *Calculate* D_c *and* D_s

$$D_c = \underbrace{\frac{3}{4}a^3\varepsilon\omega\mathbf{C}(9\omega^2\mathbf{I}+\mathbf{A^2})^{-1}\mathbf{B}}_{\text{input}} \underbrace{-\varepsilon\mathbf{C}(9\omega^2\mathbf{I}+\mathbf{A^2})^{-1}(\mathbf{A^2p_3}+3\omega\mathbf{Aq_3})}_{\text{filtercore}} + \underbrace{\varepsilon\mathbf{Cp_3}}_{\text{output}}$$

$$D_s = \underbrace{\frac{1}{4}a^3\varepsilon\mathbf{C}(9\omega^2\mathbf{I}+\mathbf{A^2})^{-1}\mathbf{AB}}_{\text{input}} \underbrace{-\varepsilon\mathbf{C}(9\omega^2\mathbf{I}+\mathbf{A^2})^{-1}(\mathbf{A^2q_3}-3\omega\mathbf{Ap_3})}_{\text{filtercore}} + \underbrace{\varepsilon\mathbf{Cq_3}}_{\text{output}}.$$

   $\rightarrow$ In D_c and D_s **keep only the terms corresponding to stages of the filter that (exist and) introduce distortion**.

6) *Derive THD*

$$\text{THD} \approx 10\log_{10}\left(\frac{D_c^2+D_s^2}{S_c^2+S_s^2}\right) \quad (\text{dB}).$$

7) The individual harmonic components at the output of the filter contributed by the input stage, the filter core stage and the output stage are, respectively

$$\mathcal{D}_1 = \frac{1}{4}a^3\varepsilon\mathbf{C}(9\omega^2\mathbf{I}+\mathbf{A^2})^{-1}\left(3\omega\mathbf{B}\cos(3\omega t)+\mathbf{AB}\sin(3\omega t)\right)$$
$$\mathcal{D}_2 \approx -\varepsilon\mathbf{C}(9\omega^2\mathbf{I}+\mathbf{A^2})^{-1}\mathbf{A} \times\left((\mathbf{Ap_3}+3\omega\mathbf{q_3})\cos(3\omega t)+(\mathbf{Aq_3}-3\omega\mathbf{p_3})\sin(3\omega t)\right)$$
$$\mathcal{D}_3 = \varepsilon\mathbf{C}\left(\mathbf{p_3}\cos(3\omega t)+\mathbf{q_3}\sin(3\omega t)\right).$$

ACKNOWLEDGMENT

The authors would like to thank Profs. A. Andreou and G. Cauwenberghs and Drs. J. Georgiou and P. Pouliquen for their insightful comments and discussions. They would also like to thank F. Tejada and E. Choi for proofreading the manuscript.

REFERENCES

[1] Y. Tsividis and J. O. Voorman, *Integrated Continuous-Time Filters*. New York: IEEE, 1993.
[2] Y. Tsividis, "Intergrated continuous-time filter design—an overview," *IEEE J. Solid-State Circuits*, vol. 29, pp. 166–176, Mar. 1994.
[3] S. Willingham and K. Martin, *Integrated Video-Frequency Continuous-Time Filters*. Boston, MA: Kluwer Academic, 1995.
[4] J. E. Franca and Y. Tsividis, Eds., *Design of Analog-Digital VLSI Circuits for Telecommunications and Signal Processing*, 2nd ed, New Jersey: Prentice Hall, 1994.
[5] V. Gopinathan, Y. Tsividis, K. Tan, and R. Hester, "Design considerations for high-frequency continuous-time filters and implementation of an anti-aliasing filter for digital video," *IEEE J. Solid-State Circuits*, vol. 25, pp. 1368–1378, 1990.
[6] J. M. Khoury, "Design of a 15-MHz CMOS continuous-time filter with on-chip tuning," *IEEE J. Solid-State Circuits*, vol. 26, no. 12, pp. 1988–1997, Dec. 1991.
[7] J. Silva-Martinez, M. Steyaert, and W. Sansen, "A 10.7 MHz 68-dB SNR CMOS continuous-time filter with on-chip automatic tuning," *IEEE J. Solid-State Circuits*, vol. 27, no. 12, pp. 1843–1853, Dec. 1992.
[8] W. M. Snelgrove and A. Shoval, "A balanced 0.9 μm CMOS transconductance-C filter tunable over the VHDF range," *IEEE J. Solid-State Circuits*, vol. 27, no. 3, pp. 314–323, Mar. 1992.
[9] C.-C. Hung, K. Halonen, M. Ismail, V. Porra, and A. Hyogo, "A low-voltage, low-power CMOS fifth-order elliptic G_m-C filter for baseband mobile, wireless communication," *IEEE Trans. Circuits Syst. Video Technol.*, vol. 7, no. 4, pp. 584–593, Aug. 1997.
[10] H. Voorman and H. Veenstra, "Tunable high-frequency G_m-C filters," *IEEE J. Solid-State Circuits*, vol. 35, no. 8, pp. 1097–1108, Aug. 2000.
[11] J.-Y. Lee, C.-C. Tu, and W.-H. Chen, "A 3 V linear input range tunable CMOS transconductor and its applications to a 3.3 V 1.1 MHz chebyshev low-pass G_m-C filter for ADSL," in *IEEE Custom Integrated Circuits Conf.*, 2000.
[12] D. A. Johns and K. Martin, *Analog Integrated Circuit Design*. New York: Wiley, 1997.
[13] Y. Palaskas and Y. Tsividis, "Dynamic range optimization of weakly nonlinear, fully balanced, G_m-C filters with power dissipation constraints," *IEEE Trans. Circuits Syst. II, Analog Digit. Signal Process.*, vol. 50, no. 10, Oct. 2003.
[14] Y. Tsividis, N. Krishnapura, Y. Palaskas, and L. Toth, "Internally varying analog circuits minimize power dissipation," *IEEE Circuits Devices Mag.*, vol. 19, no. 1, pp. 63–72, 2003.
[15] Z. Y. Chang, D. Haspeslagh, J. Boxho, and D. Macq, "A highly linear CMOS G_m-C bandpass filter for video applications," in *Proc. IEEE Custom Integrated Circuits Conf.*, 1996.
[16] Y. Tsividis, M. Banu, and J. Khoury, "Continuous-time MOSFET-C filters in VLSI," *IEEE J. Solid-State Circuits*, vol. 21, no. 2, pp. 15–30, Feb. 1986.
[17] Y. Tsividis, Z. Czarnul, and S. C. Fang, "MOS transconductors and intergrators with high linearity," *Electron. Lett.*, vol. 22, pp. 245–246, Feb. 1986.
[18] F. Krummenacher and N. Johl, "A 4-MHz CMOS continuous-time filter with on-chip automatic tuning," *IEEE J. Solid-State Circuits*, vol. 23, 1988.
[19] F. Yuan and A. Opal, "Distortion analysis of periodically switched nonlinear circuits using time-varying volterra series," *IEEE Trans. Circuits Syst. I, Fundam. Theory Appl.*, vol. 48, no. 6, Jun. 2001.
[20] J. A. Cherry and W. M. Snelgrove, "On the characterization and reduction of distortion in bandpass filters," *IEEE Trans. Circuits Syst. I, Fundam. Theory Appl.*, vol. 45, no. 5, pp. 523–537, May 1998.
[21] P. Wambacq, G. Gielen, P. Kinget, and W. Sansen, "High-frequency distortion analysis of analog integrated circuits," *IEEE Trans. Circuits Syst. II, Analog Digit. Signal Process.*, vol. 46, no. 3, pp. 335–344, Mar. 1999.

[22] G. Palumbo and S. Pennisi, "High-frequency harmonic distortion in feedback amplifiers: analysis and applications," *IEEE Trans. Circuits Syst. I, Fundam. Theory Appl.*, vol. 50, no. 3, Mar. 2003.
[23] R. L. Geiger and E. Sanchez-Sinencio, "Active filter design using operational transconductance amplifiers: a tutorial," *IEEE Circuits Devices Mag.*, vol. 1, no. 2, pp. 20–32, Mar. 1985.
[24] R. Schaumann *et al.*, *Design of Analog Filters—Passive, Active RC and Switched Capacitor*. Englewood Cliffs, NJ: Prentice-Hall, 1990.
[25] N. S. Nise, *Control Systems Engineering*. New York: Wiley, 2003.
[26] T. Kato, *Introduction to Perturbation Methods*. New York: Springer-Verlag, 1995.
[27] A. S. Sedra and K. C. Smith, *Microelectronic Circuits*. New York: Oxford University Press, 1998.
[28] E. A. Coddington and N. Levinson, *Theory of Ordinary Differential Equations*. New York: McGraw-Hill, 1955.
[29] H. Khalil, *Nonlinear Systems*, 3rd ed. Englewood Cliffs, NJ: Prentice-Hall, 2002.
[30] T. Kato, *Perturbation Theory for Linear Operators*. New York: Springer-Verlag, 1985.

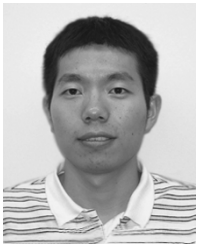

Zhaonian Zhang (S'01) received the B.S.E. degree in electronic engineering from Beijing Institute of Technology, Beijing, China, in 2001 and the M.S.E. degree in electrical and computer engineering from The Johns Hopkins University, Baltimore, MD, in 2004.

He is currently a Research Assistant with the Sensory Communications and Microsystems Lab, Johns Hopkins University. His current research interests include ultra wide-band systems, MEMS structures for acoustic systems, and digital system design.

Mr. Zhang is a member of Tau Beta Pi.

Abdullah Celik (S'02) received the B.S. degree in electrical and electronics engineering from the Bilkent University, Ankara, Turkey, in 2002, and the M.S.E. degree in electrical and computer engineering from The Johns Hopkins University, Baltimore, MD, in 2004.

He conducted research in the area of ultra-low-power VLSI systems, analog signal processing circuits, and smart adaptive sensors as a member of the Adaptive Microsystems Laboratory, Johns Hopkins University. Since 2005, he has been with Maxim Integrated Products, Sunnyvale, CA, as a member of the notebook power management IC developments team.

Paul P. Sotiriadis (M'02) received the diploma in electrical engineering and computer science from the National Technical University of Athens (NTUA), Greece, in 1994, the M.S. degree in electrical engineering from Stanford University, Stanford, CA, in 1996, and the Ph.D.degree in electrical engineering and computer science from the Massachusetts Institute of Technology, Cambridge, in May 2002.

Since June 2002, he has been an Assistant Professor with the Department of Electrical and Computer Engineering, Johns Hopkins University, Baltimore, MD. His research interests include design, optimization, and mathematical modeling of analog and mixed-signal circuits, RF and microwave circuits, fine frequency synthesis, and interconnect networks in deep-submicron technologies. He is an Associate Editor of the IEEE TRANSACTIONS ON CIRCUITS AND SYSTEMS—II: EXPRESS BRIEFS.